Title

Lipotoxic brain microvascular injury is mediated by activating transcription factor 3-dependent inflammatory and oxidative stress pathways

Journal

Journal of Lipid Research, 57(6)

ISSN

0022-2275

Authors

Aung, Hnin Hnin
Altman, Robin
Nyunt, Tun
et al.

Publication Date

2016-06-01

DOI

10.1194/jlr.m061853

Peer reviewed

Lipotoxic brain microvascular injury is mediated by activating transcription factor 3-dependent inflammatory and oxidative stress pathways

Hnin Hnin Aung,* Robin Altman,* Tun Nyunt,* Jeffrey Kim,* Saivageethi Nuthikattu,* Madhu Budamagunta,† John C. Voss,† Dennis Wilson,§ John C. Rutledge,* and Amparo C. Villablanca[1,*]

Division of Cardiovascular Medicine, Department of Internal Medicine* and Department of Biochemistry and Molecular Medicine,† School of Medicine; and Department of Pathology, Microbiology, and Immunology,§ School of Veterinary Medicine, University of California, Davis, Davis, CA 95616

Abstract Dysfunction of the cerebrovasculature plays an important role in vascular cognitive impairment (VCI). Lipotoxic injury of the systemic endothelium in response to hydrolyzed triglyceride-rich lipoproteins (TGRLs; TGRL lipolysis products) or a high-fat Western diet (WD) suggests similar mechanisms may be present in brain microvascular endothelium. We investigated the hypothesis that TGRL lipolysis products cause lipotoxic injury to brain microvascular endothelium by generating increased mitochondrial superoxide radical generation, upregulation of activating transcription factor 3 (ATF3)-dependent inflammatory pathways, and activation of cellular oxidative stress and apoptotic pathways. Human brain microvascular endothelial cells were treated with human TGRL lipolysis products that induced intracellular lipid droplet formation, mitochondrial superoxide generation, ATF3-dependent transcription of proinflammatory, stress response, and oxidative stress genes, as well as activation of proapoptotic cascades. Male apoE knockout mice were fed a high-fat/high-cholesterol WD for 2 months, and brain microvessels were isolated by laser capture microdissection. ATF3 gene transcription was elevated 8-fold in the hippocampus and cerebellar brain region of the WD-fed animals compared with chow-fed control animals. The microvascular injury phenotypes observed in vitro and in vivo were similar. ATF3 plays an important role in mediating brain microvascular responses to acute and chronic lipotoxic injury and may be an important preventative and therapeutic target for endothelial dysfunction in VCI.—Aung, H. H., R. Altman, T. Nyunt, J. Kim, S. Nuthikattu, M. Budamagunta, J. C. Voss, D. Wilson, J. C. Rutledge, and A. C. Villablanca. **Lipotoxic brain microvascular injury is mediated by activating transcription factor 3-dependent inflammatory and oxidative stress pathways. *J. Lipid Res*. 2016.** 57: **955–968.**

Supplementary key words cell signaling • diet and dietary lipids • endothelial cells • gene expression • inflammation • lipolysis • mitochondria • cerebrovascular circulation • triglyceride-rich lipoproteins • reactive oxygen species

Vascular cognitive impairment (VCI), a form of dementia caused by cerebrovascular disease, accounts for nearly 20% of cognitive dysfunction in the United States, and yet our understanding of the cerebrovascular disease processes underlying this dysfunction remains limited (1). Our understanding of vascular pathology in atherosclerotic cardiovascular disease (ASCVD) and the systemic circulation is more advanced and suggests important avenues of investigation, given the overlap of risk factors and epidemiology between ASCVD and cerebrovascular disease (2).

Epidemiological evidence suggests a diet high in saturated fat and cholesterol negatively affects the health of the vasculature and contributes to the detrimental inflammatory injury that occurs in ASCVD and cerebrovascular disease (3–8). Studies also suggest that high levels of saturated fats and cholesterol contribute to the risk of developing VCI (9–14). Chronic intermittent vascular injury, as occurs over the course of decades of consumption of high-fat meals, may significantly contribute to the long-term

This work was supported by National Institutes of Health Grants HL55667 (J.C.R.) and AG039094 (J.C.R. and A.C.V.), the Richard A. and Nora Eccles Harrison Endowed Chair in Diabetes Research (J.C.R.), the Frances Lazda Endowed Chair in Women's Cardiovascular Medicine (A.C.V.), and the University of California Davis Mouse Metabolic Phenotyping Center [National Institutes of Health Grant U24 DK092993 (J.C.R. and A.C.V.)]. Disclosures: The authors have no conflicts of interest.

Manuscript received 4 March 2016 and in revised form 11 April 2016.

Published, JLR Papers in Press, April 17, 2016
DOI 10.1194/jlr.M061853

Abbreviations: ASCVD, atherosclerotic cardiovascular disease; ATF, activating transcription factor; COX-2, cyclooxygenase-2; CP-H, 1-hydroxy-3-carboxy-2,2,5,5-tetramethylpyrrolidine; CXCL3, chemokine (C-X-C motif) ligand 3; DDIT3, DNA-damage-inducible transcript 3; EPR, electron paramagnetic resonance; GADD45A, growth arrest and DNA-damage-inducible α; HBMEC, human brain microvascular endothelial cell; HDAC9, histone deacetylase 9; HOX-1, hemeoxygenase-1; ICAM-1, intercellular adhesion molecule-1; IL, interleukin; JNK, c-Jun N-terminal kinase; KLF4, Kruppel-like factor 4; LCM, laser capture microscopy; PRNP, prion protein; qRT-PCR, quantitative RT-PCR; ROS, reactive oxygen species; SOD, superoxide dismutase; TEM: transmission electron microscopy; TGRL, triglyceride-rich lipoprotein; VCI, vascular cognitive impairment; VEGF, vascular endothelial growth factor; WD, Western diet.

[1]To whom correspondence should be addressed.
e-mail: avillablanca@ucdavis.edu

health of the cerebrovasculature through oxidative stress and inflammatory mechanisms that appear to contribute to and characterize both ASCVD and cerebrovascular disease (15, 16).

In particular, triglyceride-rich lipoproteins (TGRLs) and their lipolysis products in high physiological and pathophysiological concentrations are known to cause endothelial injury and dysfunction in the peripheral circulation. TGRLs in the blood are hydrolyzed by LPL present on endothelial cells lining the blood vessel wall (17–21). This process results in TGRL remnant particle formation and lipolysis products such as phospholipids and fatty acids. Previous studies have shown that TGRL lipolysis products cause aortic endothelial injury, including inflammation, elevated expression of reactive oxygen species (ROS), and increased vascular permeability (22–29). Additionally, activating transcription factor (ATF) 3 appears to play an important role as a master regulator of inflammation in the aortic endothelium in response to TGRL lipolysis products (22, 30). However, the effects of these lipids on brain microvascular endothelial cells of the cerebrovasculature, and their potential involvement in lipotoxic dysfunction, are unknown and have not been comprehensively studied.

The brain microvasculature differs significantly from that of the systemic circulation, particularly as relates to blood-brain barrier function. Thus, the purpose of this study was to establish the response of the brain microvascular endothelium to acute lipid challenge and investigate the hypothesis that this lipotoxic injury involves intracellular ROS and activation of the ATF3 transcriptional pathway. Additionally, we investigated whether chronic hyperlipidemia activates ATF3 upregulation in vivo. Few studies have focused on the diet-induced response of the cerebrovasculature, and a better understanding of diet-associated cerebrovascular pathology is an important goal as we pursue rational therapeutic and intervention strategies to combat VCI.

MATERIALS AND METHODS

In vitro studies

Isolation of human TGRLs. The in vitro studies utilized TGRLs isolated from human blood. The study protocol was approved by the Institutional Review Board of the University of California, Davis, and all study subjects provided informed consent. Healthy adult human volunteers consumed a moderately high-fat meal containing at least 40% fat, and postprandial (3.5 h) blood was collected by standard venipuncture (Vacutainer K_2EDTA tubes; BD, Franklin Lakes, NJ). We recruited five to six human donors/week and pooled the plasma to prepare and isolate TGRLs. The average pooled TGRL concentration was ~700–800 mg/dl. We used 150 mg/dl concentration to treat endothelial cells in our study. For experiments, we pooled TGRLs from 15 to 20 donors. Over the years, we have found the data to be very consistent using this method of collection and pooling of TGRLs. Previous studies have defined the extent and time course of triglyceride elevation following this diet and have shown triglyceride levels to be physiological to high physiological at 3.5 h (31–34). Whole blood samples were then centrifuged at 3,000 rpm for 15 min at 4°C, and the plasma fraction was collected. Sodium azide was added to the plasma as a preservative, and the plasma adjusted with mock plasma solution (ρ = 1.0063 NaCl, KBr, and EDTA). TGRLs were isolated from the plasma by ultracentrifugation at 40,000 rpm for 18 h at 14°C, and dialyzed in Spectra/Por® membrane tubing (molecular weight cutoff 3,500 g/mol; Spectrum Medical Industries, Los Angeles, CA) at 4°C overnight against a saline solution containing 0.01% EDTA. Triglyceride levels were measured using the Triglyceride Determination Kit (Sigma, St. Louis, MO).

In vitro culture and exposure of human brain microvascular endothelial cells to TGRLs. Human brain microvascular endothelial cells (HBMECs) were obtained from Angio-Proteomie (Boston, MA) and cultured in EGM™-2MV BulletKit™ containing 5% serum (CC-3202; Lonza, Walkersville, MD) in a 37°C incubator with a humidified 5% CO_2 and 95% air environment. Medium was changed every other day until 90% confluency, and cells were used at passage 5-6. One hour prior to experiments, cell culture medium was changed to fresh medium. HBMECs were then subjected to the following treatments: media alone, TGRLs alone (150 mg/dl), TGRLs hydrolyzed with LPL (referred to as TGRL lipolysis products; 150 mg/dl TGRLs plus 2 U/ml LPL for 30 min at 37°C prior to addition to the cells), or LPL alone in equivalent concentration (2 U/ml). LPL (catalog number L2254) was obtained from Sigma.

Transmission electron microscopy and Oil Red O staining of lipid droplets. Ultrastructural abnormalities in response to lipid injury in HBMECs were assessed by transmission electron microscopy (TEM). HBMECs were grown to confluence in Lab-Tek Permanox 8-well chamber plates and treated (n = 3 per treatment group) with media or TGRL lipolysis products for 3 h. After treatment, cells were washed with complete media and fixed in Karnovsky's fixative overnight. Samples were postfixed in OsO_4, embedded in epon/aryldite, and thin sections mounted on electron microscopy grids by the Electron Microscopy Imaging Facility at the University of California, Davis. Sections were examined with a Philips CM120 transmission electron microscope (Pleasanton, CA). Images were acquired digitally. For Oil Red O visualization of lipid droplets in HBMECs, cells were fixed with 4% paraformaldehyde, stained with Oil Red O, and counterstained with CAT Hematoxylin (#CATHE; Biocare Medical, Concord, CA). Cells were then mounted on slides with ProLong Gold antifade reagent (Life Technologies, Carlsbad, CA) and imaged using a Zeiss AxioObserver, LSM 700 microscope.

Electron paramagnetic resonance spin trapping of superoxide radical ($O_2^{\cdot -}$). To detect $O_2^{\cdot -}$ production by HBMECs, measurements of supernatant $O_2^{\cdot -}$ levels were performed on cells treated for 15 min with media, TGRL lipolysis, TGRL lipolysis plus superoxide dismutase (SOD) (catalog number S5395; Sigma) at 500 U/ml or Mito-TEMPO (#ALX-430-150-M005; ENZO Life Sciences, Farmingdale, NY) at 25 nM. Each treatment condition also contained 0.5 mM 1-hydroxy-3-carboxy-2,2,5,5-tetramethylpyrrolidine (CP-H) spin trap (35). Spin traps are capable of rapidly trapping free radicals such as $O_2^{\cdot -}$ to form more persistent radicals (spin adducts) detectable by electron paramagnetic resonance (EPR). Conversion of the diamagnetic hydroxy-amine CP-H (#ALX-430-078, ENZO Life Sciences) to the paramagnetic nitroxide was measured using a JEOL JES TE-100 EPR spectrometer. All spectra were obtained at room temperature by averaging two 2 min scans with a sweep width of 100 G at a microwave power of 3 mW and modulation amplitude optimized to the natural line width of the spin probe.

Mitochondrial superoxide radical generation. To assess the origin of the superoxide generation in HBMECs, cells were grown to confluence on 12 mm round glass coverslips coated with Attachment

Factor™ (4Z0-210S; Cell Systems, Kirkland, WA), placed in 24-well medical-grade polystyrene plates (BD Falcon, San Jose, CA), and treated (n = 3 coverslips per treatment group) with media, TGRL lipolysis, or TGRL lipolysis plus the mitochondria-specific superoxide radical scavenger Mito-TEMPO (25 nM) for 15 min. After treatment, cells were washed with Krebs-HEPES buffer and incubated with Mito-SOX™ and Mito-Tracker® in Krebs-HEPES buffer for 20 min at 37°C according to the manufacturer's protocol. MitoSOX Red Mitochondrial Superoxide Indicator (M36008) and MitoTracker Green FM (M-7514) were purchased from Molecular Probes (Eugene, OR). Nuclei were stained with 4',6-diamidino-2-phenylindole (DAPI), and the production of superoxide by mitochondria was visualized by deconvolution fluorescence microscopy (Applied Precision LLC, Issaquah, WA).

Quantitative RT-PCR analysis of gene transcription. Total RNA was extracted from HBMECs in 6-well plates treated with media, LPL, TGRLs, or TGRL lipolysis products using the RNeasy Mini Kit (Qiagen) including the DNA digestion step as described by the manufacturer. An aliquot equivalent to 5 μg of total RNA extracted from each sample was reverse-transcribed to obtain cDNA in a final volume of 20 μl consisting of buffer, random hexamers, DTT, deoxynucleoside triphosphates, and SuperScript® III First-Strand Synthesis System (Invitrogen). Quantitative RT-PCR (qRT-PCR) with SYBR as fluorescent reporter was used to quantify the expression of selected genes identified by GeneChip analysis. Specific human primers were designed with Primer Express 1.0 software (Applied Biosystems) using the gene sequences obtained from previously published Affymetrix Probeset IDs (**Table 1**) (22). Reactions were carried out in 384-well optical plates containing 25 ng RNA in each well. The quantity of applied RNA was normalized by simultaneously amplifying cDNA samples with GAPDH-specific primers. Transcript levels were measured by RT-PCR using the ABI Vii7 Sequence detection system (PE Applied Biosystems, Foster City, CA). The PCR amplification parameters were initial denaturation step at 95°C for 10 min followed by 40 cycles, each at 95°C for 15 s (melting), and 60°C for 1 min (annealing and extension). A comparative threshold cycle (Ct) method was used to calculate relative changes in gene transcription determined from real-time quantitative PCR experiments [Applied Biosystems user bulletin no. 2 (P/N4303859)] (36). The Ct, which correlates inversely with the target mRNA levels, was measured as the cycle number at which the SYBR Green emission increases above a preset threshold level. The specific mRNA transcripts were expressed as fold difference in the transcription of the specific mRNAs in RNA samples from the TGRL lipolysis-treated cells compared with those from the control-treated cells.

TABLE 1. Oligonucleotide sequences for each human primer were custom prepared using the Affymetrix Probeset IDs

Gene	Primer Sequence (5′-3′)
GAPDH	Sense-CACCAACTGCTTAG
	Antisense-TGGTCATGAGTCCT
SOD-1	Sense-TCATCAATTTCGAGCAGAAGGA
	Antisense-TTCCCCACACCTTCACTGGT
SOD-2	Sense-GGGAATACCCCAGTTGTGAAAG
	Antisense-TGGTGTCAGATGTTGCCTTACAG
SOD-3	Sense-CACTGTGTTGTCACTGGGCG
	Antisense-CCCACCGTGAAGATCCAATG
HOX-1	Sense-TCTTCCCCAACGAAAAGCAC
	Antisense-CCCCCTCTGAAGTTTAGGCC
COX-2/PTGS2	Sense-CTGAATGTGCCATAAGACTGACCT
	Antisense-TCCACAGATCCCTCAAAACATTT
ATF3	Sense-TTCTCCCAGCGTTAACACAAAA
	Antisense-AGAGGACCTGCCATCATGCT
ATF4	Sense-GTGGCATCTGTATGAGCCCA
	Antisense-GGCTGTGCTGAGGAGACCC
DDIT3	Sense-AGAGTGGTCATTCCCCAGCC
	Antisense-CTTTCTCCTTCATGCGCTGC
PRNP	Sense-GGAAACCCTTTTGCGTGGT
	Antisense-GAAACGATTCAGTGCACATTGTAAG
HDAC9	Sense-TTTAATCAAGAAACTACCTGGAACCA
	Antisense-ATTTAAGTCCAGCTTTCCTTTTCACT
GADD45A	Sense-GGCCCGGAGATAGATGACTTT
	Antisense-CCTTCTTCATTTTCACCTCTTTCC
E-selectin	Sense-TGGCAATGAAAAATTCTCAGTCA
	Antisense-TCAAGGCTAGAGCAGCTTTGG
ICAM-1	Sense-CAGAAGAAGTGGCCCTCCATAG
	Antisense-GGGCCTTTGTGTTTGATGCTA
KLF4	Sense-ACTGGAAGTTGTGGATATCAGGG
	Antisense-CTCCCCCAACTCACGGATATAA
VEGF	Sense-AGCTCTGCCCTCCCCG
	Antisense-CTTTCAAAGGAATGTGTGCTGG
CXCL3	Sense-TAGGGACAGCTGGAAAGGGA
	Antisense-ACCCTCGTAAGAAATAGTCAAACACAT
IL-1α	Sense-GTTTTATCATTTTCAAAATGGAGGG
	Antisense-TGCGGCAGGAAGGCTTAG
IL-8	Sense-CCTTTCCACCCCAAATTTATCA
	Antisense-TGGTCCACTCTCAATCACTCTCAG
IL-6	Sense-CTGCGCAGCTTTAAGGAGTTC
	Antisense-TTGCCGAAGAGCCCTCAG
JunB	Sense-AATGGAACAGCCCTTCTTACCACGA
	Antisense-GGCTCGGTTTCAGGAGTTTGTAGT

COX-2, cyclooxygenase-2; CXCL3, chemokine (C-X-C motif) ligand 3; DDIT3, DNA-damage-inducible transcript 3; GADD45A, growth arrest and DNA-damage-inducible α; HOX-1, hemeoxygenase-1; PRNP, prion protein; HDAC9, histone deacetylase 9; ICAM-1, intercellular adhesion molecule-1; IL, interleukin; KLF4, Kruppel-like factor 4; PTGS2, prostaglandin-endoperoxide synthase 2; VEGF, vascular endothelial growth factor. The human primers were used as described in the Materials and Methods.

Western blotting. To confirm translation of ATF3 mRNA, we performed Western blot analysis. For these experiments, HBMECs were grown to confluence in 6-well plates and then treated for 3 h with media, LPL, TGRLs, or TGRL lipolysis products. After the incubation, cells were washed twice with PBS, scraped with cold PBS, and centrifuged at 3,000 rpm for 10 min at 4°C. Cell pellets were lysed in RIPA buffer containing 50 mM Tris (pH 7.4), 150 mM NaCl, 1% NP40, 0.25% sodium deoxycholate, 0.1% SDS, 1× Protease inhibitor cocktail set 1 (Calbiochem, La Jolla, CA), 1 mM NaF, and 1 mM $Na3VO_4$. Protein concentration was determined with the bicinchoninic acid assay (Pierce), and equal amounts of proteins (60 μg) were separated by NuPAGE® Novex® 4–12% Bis-Tris protein gels using NuPAGE® MES SDS Running Buffer (Life Technologies, Grand Island, NY). Proteins then were transferred onto 0.2 μm polyvinylidenedifluoride membranes (Bio-Rad, Hercules, CA), which were subsequently blocked with 5% nonfat milk for 1 h and probed with ATF3 (1:200 dilution), c-Jun (1:200 dilution), phosphorylated c-Jun N-terminal kinase (p-JNK) antibody (1:1,000 dilution), phosphorylated c-Jun (p-c-Jun; 1:1,000), JNK1 (1:1,000), ATF4 (1:1,000), c/EBP homologous protein (1:1,000), and cleaved caspase-9 (1:1,000) or blotting control mouse monoclonal anti-β-actin (1:5,000) at 4°C overnight. Membranes were then incubated with HRP-conjugated secondary anti-rabbit or anti-mouse antibody (1: 5,000–10,000). Blots were developed with the enhanced chemiluminescence detection system according to the manufacturer's instructions (Amersham). Protein expression levels were determined using a densitometer and Image Quant.

Antibodies were purchased from the following sources: monoclonal anti-β-actin antibody (A 5441) from Sigma; ATF3 (sc-188) and c-Jun (sc-1694) from Santa Cruz Biotechnology (Santa Cruz, CA); c/EBP homologous protein (#2895), p-c-Jun (#9261), p-JNK (#9251), JNK1 (2C6, #3708), and ATF4 (D4B8, #11815) caspase-9 (#9502), and cleaved caspase-9 (Asp330, #9501) from Cell Signaling

Technology (Danvers, MA); and HRP-conjugated secondary anti-mouse (Amersham #NXA931) and anti-rabbit antibody (Amersham #NA9340V) from GE Healthcare Life Sciences (Pittsburgh, PA). Secondary goat anti-rabbit antibody conjugated to Alexa Fluor 488 (A-11034) was purchased from Molecular Probes.

ATF3 siRNA experiments. To further investigate involvement of the ATF3 signaling pathway activated by lipolysis products, cells were pretransfected with scrambled or ATF3 siRNA prior to treatment with lipolysis products. Scrambled and negative control siRNA (AM4611) and ATF3 siRNA (Gene Bank: NM_001030287, AM16810, siRNA ID-241437) were purchased from Ambion (5′-AAGUGCCGAAACAAGATT-3′; 3′-UCUUCUUGUUUCGGCACUUTG-5′) (Carlsbad, CA). A different construct of ATF3 siRNA (5′-GCAUUAUUGGAUGUCAAUAGCAUTG-3′; 3′-AUCGUAAUAACCUACAGUUAUCGUAAC-5′) and IDT TriFECTa® kit Duplex1 were purchased from Integrated DNA Technologies Inc. (IDT; Coralville, IA). HBMECs were cultured and treated with lipolysis products for 3 h in 6-well plates. Cells were pretransfected for 18 h with 5 nM ATF3 siRNA or negative control (scrambled) siRNA in media without serum using HiPerfect reagent (Qiagen) according to the manufacturer's protocol. Cells were transfected with two independent ATF3 siRNA constructs from IDT and Ambion. siRNA-transfected cells were exposed to lipolysis products for 3 h as outlined above, and transcription of selected genes was assessed by qRT-PCR. PCR primers were obtained from Operon (Huntsville, AL). To determine the ATF3 signaling pathway activated by TGRL lipolysis products, ATF3, ATF4, p-c-Jun, and c-Jun protein expression was analyzed by Western blotting according to the protocol described above.

Immunofluorescence analysis of nuclear ATF3 accumulation. To determine the extent of ATF3 nuclear accumulation in response to TGRL lipolysis products, HBMECs were grown to confluence on 12 mm round glass coverslips coated with attachment factor, placed in 24-well medical-grade polystyrene plates, and treated (n = 4 coverslips per treatment group) with media, TGRLs, TGRL lipolysis products, or LPL for 3 h. After treatment, HBMECs were fixed with 4% paraformaldehyde in PBS for 30 min at room temperature and then washed 3× with PBS. Cells were then permeabilized, blocked, and incubated with rabbit polyclonal anti-ATF3 (1:100 dilution, catalog number sc-188, Santa Cruz Biotechnology) as previously described (22). Subsequently, cells were treated with goat anti-rabbit secondary antibody conjugated to Alexa Fluor 488 (Molecular Probes), and the nuclei were counterstained for 5 min with DAPI (1 μg/ml). After cells were mounted on slides, they were evaluated and photographed with an Olympus Provis system fluorescence microscope (Waltham, MA). Images are representative of at least five separate experiments.

Caspase-3/7 apoptosis assays. Endothelial cell apoptosis was measured by caspase-3/7 activation using the Apo-ONE® Homogeneous Caspase-3/7 Assay kit (Promega, Madison, WI) according to the manufacturer's instructions. HBMECs were grown to confluence on 96-well plates and treated with media, LPL, TGRLs, or TGRL lipolysis products for 3 h. After incubation, caspase-3/7 activity was measured using the Caspase-3/7 Assay kit. The samples were measured by a fluorescence microplate reader (SpectraMax F5; Molecular Devices, Sunnyvale, CA) with a 485 nm excitation filter and a 530 nm emission filter. Additionally, caspase-3/7 activity was measured in cells pretransfected with ATF3 siRNA for 18 h and then treated with lipolysis products for 3 h.

In vivo studies

Chronic lipid injury in wild-type and apolipoprotein $E^{-/-}$ mice. The apolipoprotein $E^{-/-}$ (apo$E^{-/-}$) mouse on the C57BL/6J background (strain B6.129P2-Apoe^{tm1Unc}/J, stock 002052, from Jackson Laboratories, Bar Harbor, ME) fed a Western diet (WD) has increased triglycerides, cholesterol, and fatty acids and, as such, exhibits characteristic vascular inflammation and development of human-like aortic atherosclerotic lesions (37, 38). We utilized this well-characterized model of aortic inflammation as a suitable model to assess inflammation in brain microvessels. Wild-type C57BL/6J mice (stock 000664 from Jackson Laboratories) were also used for this study as genetic controls. Animals were housed in a temperature- and humidity-controlled environment with a 12 h light/dark cycle in the University of California, Davis Mouse Biology Program. Research was conducted in conformity with the Public Health Service Policy on Humane Care and Use of Laboratory Animals, and all protocols were approved by the Institutional Animal Care and Use Committee of the University of California, Davis. For these studies, 6-week-old male mice were fed a standard chow (n = 7–9 mice; Nestlé Purina PetCare Co., St. Louis, MO) or WD (n = 7–15 mice; catalog no. 88137, Harlan Laboratories, Madison, WI) composed of 21% fat and 0.2% cholesterol (w/w) for an additional 6–8 weeks. This length of time has been previously shown to be sufficient for atheroma development (38) and resulted in atherosclerotic lesions in our system that were moderately advanced per the classification of Stary (39–41). Mean weight of the animals at baseline was 23 g and increased by an average of 26% in mice on the WD compared with 13% on the chow diet.

Isolation of murine brain segments. After chow or lipid feeding, wild-type and apo$E^{-/-}$ mice were euthanized by exsanguination between the hours of 10 AM and 2 PM during the light phase of their light/dark cycle, and intravascularly perfused by retrocardiac perfusion with diethylpyrocarbonate-treated PBS under anesthesia [intraperitoneal Nembutal (0.6% solution, 120–180 mg/kg of body weight) or xylazine/ketamine (2.31 mg/ml xylazine/20.8 mg/ml ketamine solution, 0.0185–0.0208 mg xylazine and 0.166–0.187 mg ketamine per gram of body weight)]. Intact brains of chow- and lipid-fed mice were rapidly removed and cut into frontal, temporal, occipital, and cerebellar segments, embedded in HistoPrep Frozen Tissue Embedding Media (Fisher Scientific, Pittsburgh, PA), and tissue blocks stored at −80°C. Brain segments were coronally cryosectioned at 8 μm thickness, and each section was placed on a charged RNA-free PEN Membrane Glass Slide. RNA*later*®-ICE (Life Technologies) was added to each section to prevent RNA degradation, and sections were stored at −80°C until use.

Visualization of hippocampal region. To identify the hippocampus and hippocampal neurons, brain sections in the medial aspect of the temporal lobe of study mice were stained with hematoxylin and visualized with microscopy by a histopathology expert and study coauthor (D.W.). Microvessels within the hippocampal tissue were identified with alkaline phosphatase staining utilizing 5-bromo-4-chloro-3-indolyl phosphate/nitro blue tetrazolium chloride (BCIP/NBT) substrate as previously described (42).

Laser capture microdissection and qRT-PCR analysis of ATF3 gene transcription in murine brain microvessels. For analysis of ATF3 gene transcription of brain microvessels, we utilized laser capture microdissection (LCM). For LCM, brain tissue sections from the frontal, temporal, hippocampal, and cerebellar segments of chow- and lipid-fed apo$E^{-/-}$ mice were submerged in nuclease-free water and dehydrated in desiccant. Laser capture was performed of the entire vessel wall of brain microvessels in the cryosections under direct microscopic visualization using a Leica LMD6000 Laser Microdissection Microscope (Leica Microsystems, Wetzlar, Germany). Vessels were chosen for laser capture on the

basis of their morphology and size (25–250 μm in diameter). Total RNA was extracted from the laser-captured brain microvessels and amplified using an Arcturus® RiboAmp® HS PLUS RNA Amplification Kit (Life Technologies) according to the manufacturer's instructions. The integrity and quality (RIN ⩾7) of the RNA from LCM-derived vessels was assessed by a scrape test using the protocol provided in the kit and verified up to 90 min postmicrodissection using an Agilent 2100 Bioanalyzer (Agilent Technologies, Santa Clara, CA). The integrity of the RNA was also verified by agarose gel electrophoresis of the RT-PCR products. Total RNA samples extracted and amplified from the laser-captured brain microvessels were used to analyze transcription of ATF3 and normalized to GAPDH transcription. The murine primers used are detailed in **Table 2.**

Statistical methods. Results are expressed as means ± SEM, unless otherwise indicated. Student's *t*-tests were performed to analyze gene transcription in brain regions between the WD-fed apoE$^{-/-}$ and chow-fed apoE$^{-/-}$ animals. Unpaired Student's *t*-tests or two-way ANOVA with repeated measures were used for comparisons between treatments in the in vitro experiments. Statistical analyses were performed using Excel (Microsoft, Redmond, WA), SigmaStat (Systat Software Inc., San Jose, CA), or GraphPad PRISM 5.0 software (San Diego, CA), and significance was determined at $P \leqslant 0.05$.

RESULTS

TEM reveals ultrastructural abnormalities in human brain microvascular cells treated with TGRL lipolysis products

We first sought to determine the characteristics of acute lipid-induced injury in the human brain microvascular endothelium. When HBMECs were treated with TGRL lipolysis products, electron microscopy revealed two striking abnormalities (**Fig. 1A**). Mitochondria were dilated with spaces separating cristae often containing flocculant lightly electron-dense material, and media-treated control mitochondria were elongated and tubule shaped. Additionally, the cells rapidly formed spherical electron-dense inclusions interpreted to be lipid droplets. These were often found in close proximity to mitochondria. We used Oil Red O staining to further confirm the presence of lipid in the inclusions in the lipolysis product-treated group (Fig. 1B).

TABLE 2. Oligonucleotide sequences for each murine primer were obtained from the Affymetrix database using Probeset IDs and Primer3 software

Gene	Primer Sequence (5′-3′)
GAPDH	Sense-GCAACAGGGTGGTGGACCT
	Antisense-GGATAGGGCCTCTCTTGCTCA
ATF3	Sense-ATCGTGGGCCGCTCTAGGCACC
	Antisense-CTCTTTGATGTCACGCACGATTTC
IL-1α	Sense-CCACGAAGCTCTCCGTACAT
	Antisense-GCTTTAAGGACGGGAGGGAG
IL-1β	Sense-GTTGATTCAAGGGGACATTA
	Antisense-AGCTTCAATGAAAGACCTCA
TNF-α	Sense-GCTCCCAGAAAAGCAAGCAG
	Antisense-CATCTTTTGGGGGAGTGCCT
JNK1/MAPK8	Sense-TTTTGCTGTGAAACTTTTGATTATCA
	Antisense-AACTTAACATGTGGTGCAATTTCTGT
S100B	Sense-GACTCCAGCAGCAAAGGTGA
	Antisense-ATCTTCGTCCAGCGTCTCCA
IL-11	Sense-TCTCTTCAGACCCTCGAGCA
	Antisense-CATGCCGGAGGTAGGACATC
JUNB	Sense-CAGCTCAAGCAGAAGGTCATGA
	Antisense-CAGCAACTGGCAGCCGTT
COX-2	Sense-CTTAGTTCCGTTTCTCGTGGTCA
	Antisense-AACCCAATCAGCGTTTCTCG
CAS3	Sense-TGCTAGAAACGAAAGGGCCA
	Antisense-TTGCTGGATGCTTTCCAAGTC
CAS7	Sense-CTGCCTGAGATGGAAACCAAG
	Antisense-GGAGGCCTTTGGTGTCTGACT
CAS9	Sense-ACATGCAGTTGTGGGCGTT
	Antisense-GTGAGTCCCAGCCTCAAAACA

CAS, caspase. The murine primers were custom prepared and used as described in the Materials and Methods.

Increased levels of superoxide radical generation from TGRL lipolysis product-treated HBMECs originate from mitochondria

Lipid-induced injury to HBMECs is thought to be related to the production of ROS. We investigated the involvement of oxidative stress in the observed cellular injury resulting from acute lipid insult by determining the levels of lipid-induced ROS produced by HBMECs. EPR spectroscopy was used to measure the conversion of the diamagnetic CP-H spin trap to its stable paramagnetic nitroxide spin adduct by ROS. As shown in **Fig. 2A**, exposure of HBMECs to TGRL lipolysis products generates a large nitroxide signal, indicating an oxidation of the CP-H spin trap. The nitroxide signal is substantially reduced by the simultaneous addition of SOD, which catalyzes the conversion of superoxide into oxygen and hydrogen peroxide. The intensities of the EPR signals are quantified in Fig. 2B. A statistically significant reduction (nearly 50%) in nitroxide signal is obtained when cells are treated with both TGRL lipolysis products and 500 U/ml SOD, suggesting superoxide represents the major reactive species produced in response to lipolysis products.

To probe the origin of the ROS, HBMECs were stained with both a mitochondria-specific green fluorescent probe (MitoTracker Green) and a MitoSOX probe that undergoes oxidation and fluoresces red upon contact with mitochondrial superoxide. Colocalization of superoxide and mitochondria was revealed by orange coloration. As seen in Fig. 2C, following treatment with lipolysis products, HBMECs displayed bright orange staining dispersed throughout the cytoplasm, compared with a notable lack of orange staining in the cells treated with media alone. Mito-TEMPO, a mitochondria-specific superoxide scavenger, attenuates the lipolysis product-induced increase in superoxide. This implicates a mitochondria-mediated pathway in the superoxide production following acute lipid injury in HBMECs.

TGRL lipolysis products activate genes involved in oxidative stress, transcription factor, and proinflammatory activities

Our previous systems biology work demonstrated induction of proinflammatory responses by TGRL lipolysis products in HBMECs, and involvement of ATF3 as a principal response gene (43). HBMEC gene transcription following TGRL lipolysis product treatment for up to 3 h was determined by qRT-PCR analysis. **Fig. 3A–C** shows significantly increased transcription of oxidative stress, transcription factor, and proinflammatory response genes. Oxidative

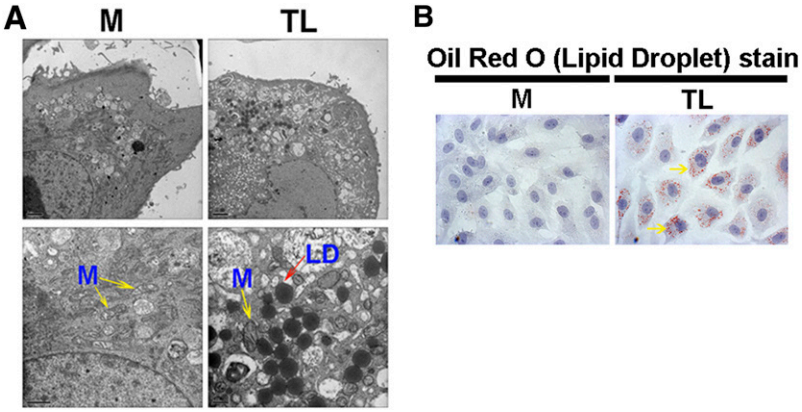

Fig. 1. TGRL lipolysis products induced mitochondrial dysfunction and lipid droplet (LD) formation. HBMECs were treated with media control (Media) or TGRL lipolysis products (TL, 150 mg/dl + LPL, 2 U/ml) for 3 h. A: TEM image of swollen mitochondria (M, yellow arrows) and adjacent lipid droplets (LD, red arrow). Original magnification 8,400× (bar = 1 μm). B: LD formation (yellow arrows) was observed in TGRL lipolysis product-treated cells by Oil Red O staining (bar = 40 μm). n = 3/treatment group.

stress response genes, including mitochondrial SOD-2, HOX-1, and COX-2, were significantly upregulated by TGRL lipolysis products (Fig. 3A). In contrast, soluble SOD-1 and extracellular SOD-3 were not changed.

Lipolysis products activated genes encoding transcription factors, including ATF3, DDIT3, ATF4, PRNP, HDAC9, and GADD45A (Fig. 3B). In particular, lipolysis product-treated HBMECs expressed increased levels of ATF3 (nearly 75-fold compared with media control, $P \leq 0.05$) after 3 h of treatment. Proinflammatory genes activated included E-selectin, ICAM-1, KLF4, VEGF, CXCL3, IL-1α, IL-8, and IL-6 (Fig. 3C). There were no significant differences between the media control and TGRL-treated or LPL-treated control groups at any time point.

TGRL lipolysis products increase protein expression of ATF3, ATF4, p-c-Jun, and cleaved caspase-9 and increase ATF3 nuclear accumulation in HBMECs

To further determine the signaling pathway(s) responding to the lipid-induced injury, we probed protein expression of ATF3, and observed significantly ($P \leq 0.05$) increased levels after 3 h of lipolysis product treatment (**Fig. 4A**). Fig. 4B, D also shows elevated protein levels of ATF4 and p-c-Jun. However, p-JNK protein levels did not change (Fig. 4C). Lipolysis product treatment also resulted in increased ATF3 nuclear accumulation (Fig. 4E), indicative of activation of the transcription factor within 3 h of exposure to the lipid.

Caspase-9 activity has been linked to the mitochondrial death pathway; thus, we investigated levels of cleaved caspase-9 indicative of conversion of procaspase-9 to the active form that upregulates downstream apoptotic cascades. As shown in Fig. 4F, cleaved caspase-9 (37 kDa) protein displays an increasing trend after treatment with lipolysis products for 1 h. In separate experiments, protein expression for ATF3, ATF4, and cleaved caspase-9 (37 kDa) was shown to be dependent on time (1 h to 3 h) of incubation with the lipolysis products (data not shown).

ATF3 siRNA suppresses induction of a subset of transcription factors and proinflammatory response genes

As shown in **Fig. 5A**, knockdown by ATF3 siRNA resulted in a significant 63% reduction in ATF3 gene transcription ($P \leq 0.05$). Concurrent with the decrease in ATF3 transcript, we also observed varying effects on TGRL lipolysis product-induced genes (Fig. 5B, C). In particular, ATF3 siRNA significantly decreased gene transcript levels of the proinflammatory genes E-selection, ICAM -1, KLF4, and CXCL3 and significantly upregulated levels of IL-1α and the oxidative stress gene HOX-1 ($P \leq 0.05$).

ATF3 siRNA also differentially affected protein levels of transcription factors involved in the lipolysis product-induced signaling pathway. **Fig. 6A** shows significantly reduced protein levels of ATF3 protein following pretreatment with ATF3 siRNA ($P \leq 0.05$). Additionally, ATF3 knockdown resulted in decreased levels of ATF4 (Fig. 6B) and increased levels of p-c-Jun (Fig. 6C).

Elevated levels of proapoptotic factors in TGRL lipolysis product-treated HBMECs are attenuated by ATF3 siRNA

We then sought to determine how disruption of the ATF3 signaling pathway by knockdown with ATF3 siRNA would affect apoptotic injury in HBMECs treated with lipolysis products. Caspase-3/7 activation occurs downstream of procaspase cleavage and activation and results in the cleavage of many caspase substrates that eventually effect the final steps of the apoptotic cascade. Lipolysis products induced significantly increased caspase-3/7 activity (Fig. 6D) that was attenuated by pretreatment with ATF3 siRNA (Fig. 6E).

ATF3 gene transcription is increased by WD in brain vasculature of apoE$^{-/-}$ mice

As our in vitro cell studies demonstrated marked endothelial effects of acute lipid injury induced by TGRL lipolysis products, we then sought to determine whether chronic exposure to a high-fat lipid challenge would produce analogous deleterious vascular effects in an in vivo apoE$^{-/-}$ animal model. We investigated ATF3 gene transcription in murine brain blood vessels isolated by LCM from wild-type and apoE$^{-/-}$ mice fed either the WD or chow and the hippocampal and other brain regions of apoE$^{-/-}$ mice fed chow diet (**Fig. 7**). As shown in Fig. 7, transcription of ATF3 in brain vasculature was 8-fold higher ($P \leq 0.001$) in WD compared with chow diet in apoE$^{-/-}$ mice. In addition, regional analysis showed that ATF3 transcription in brain vasculature was restricted to the hippocampus and cerebellum, as ATF3 transcription was not significantly increased in the frontal or temporal lobes of WD-fed

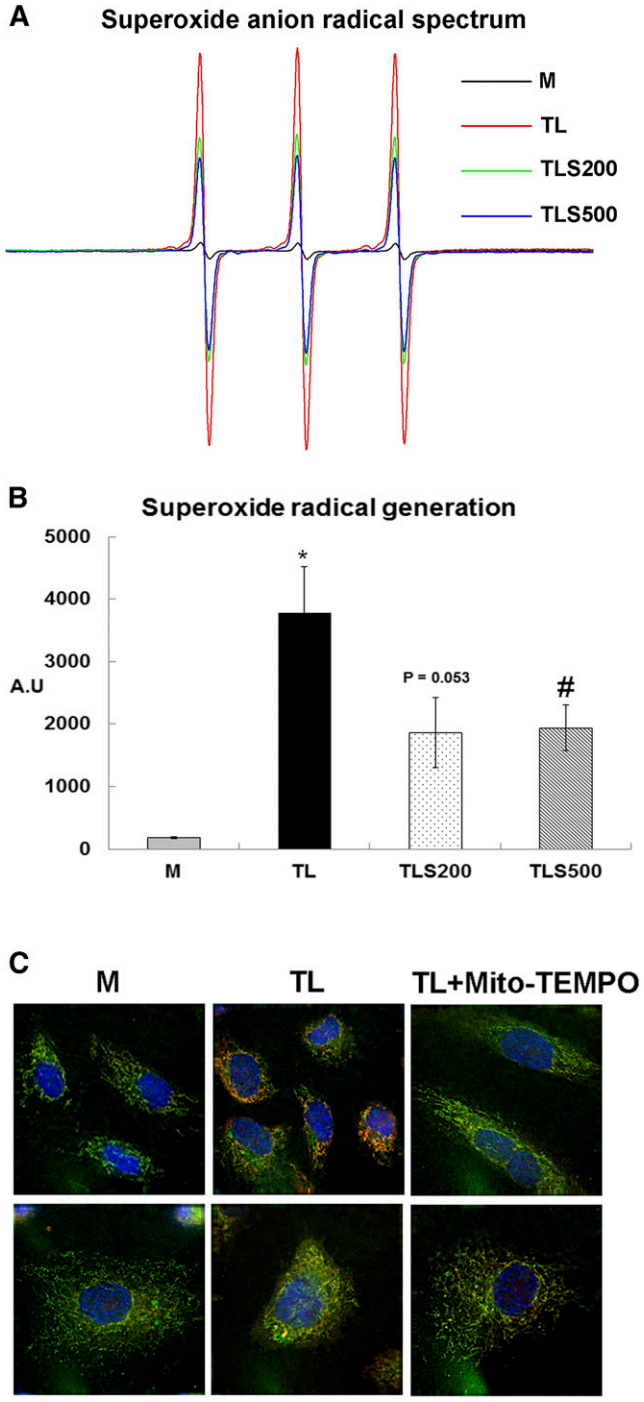

Fig. 2. TGRL lipolysis product-activated superoxide radical ($O_2^{\cdot-}$) generation was suppressed by SOD or Mito-TEMPO. HBMECs were treated for 15 min with media (M), TGRL lipolysis products (TL), TGRL lipolysis products plus SOD (TLS, 500 U/ml SOD), or TGRL lipolysis products plus Mito-TEMPO (25 nM). A: Oxidation of the CP-H spin trap measured by EPR spectroscopy. Supernatant solutions from the alternatively treated cells were incubated with the diamagnetic (EPR silent) CP-H spin trap and scanned by EPR. The intensity of the three-line nitroxide spectrum is indicative of the rate of CP-H oxidation, which generates the paramagnetic nitroxide species. Addition of SOD to the sample reduces the nitroxide signal by ~50%, indicating superoxide as a major species in CP-H oxidation. Quantification of oxidized CP-H signal is shown in B. C: Superoxide radical generation in mitochondria was suppressed by Mito-TEMPO. Cells were stained with MitoTracker (green) for mitochondria and MitoSox (red) for mitochondrial superoxide generation. Orange color represents colocalization of superoxide radical production in mitochondria. n = 4–5/treatment group, and results expressed as means ± SEM. $P \leq 0.05$ was considered significant. * = TL compared with M; # = 500 U/ml SOD (TLS500) compared with TL.

apoE$^{-/-}$ mice versus chow-fed apoE$^{-/-}$ mice. There was no increase or difference in ATF3 transcription between WD and chow in wild-type mice. In addition, the high fat diet-induced vascular damage on the brain was not accompanied by any obvious observable damage to neurons or glia by H and E staining.

DISCUSSION

The pathophysiological mechanisms of cerebrovascular dysfunction are poorly understood; although strong correlative data exist linking blood lipids to cerebrovascular injury (9–14, 44, 45), little is known regarding the mechanisms of lipid-induced cerebrovascular injury, which could have relevance to prevalent health conditions such as VCI and Alzheimer's disease. Lipotoxicity results from intracellular accumulation of excess lipid, particularly fatty acids, in nonadipose tissue leading to lipid imbalance, cellular dysfunction, and cell death (46–48). Our work indicates for the first time that TGRL lipolysis products cause lipotoxic injury to HBMECs in vitro. This lipotoxicity occurs through stimulation of mitochondrial metabolism toward overproduction of superoxide radical, which drives both ATF3-mediated inflammatory and apoptotic responses, and cellular ROS adaptation. Our findings also have relevance in vivo, as we further demonstrated ATF3 is upregulated in brain microvessels in a murine model of hyperlipidemia, and a similar overall in vivo phenotype to that observed in vitro in HBMECs. These responses may ultimately affect the integrity of the blood-brain barrier, induce neurovascular inflammation, and contribute to cognitive decline.

Our previous studies indicated acute exposure to hydrolyzed TGRLs (TGRL lipolysis products) lead to inflammatory injury in human aortic endothelial cells (22, 23, 27, 28), and we hypothesized similar effects may occur in the vasculature of the brain. In our in vitro model of cultured HBMECs, TEM revealed ultrastructural abnormalities in response to TGRL lipolysis products indicative of lipotoxic injury, including mitochondrial swelling and increased levels of lipid droplets in close proximity to mitochondria at 3 h. To further investigate the particular pathway responsible for this injury, we assayed for production of ROS and detected notably elevated levels of superoxide within 15 min of TGRL lipolysis product treatment that were significantly reduced by concomitant treatment with SOD, suggesting that TGRL lipolysis product-mediated HBMEC injury is dependent, at least in part, on elevated ROS. Immunofluorescent staining of cells treated with lipolysis products and the mitochondria-specific antioxidant Mito-TEMPO demonstrated the superoxide originated from

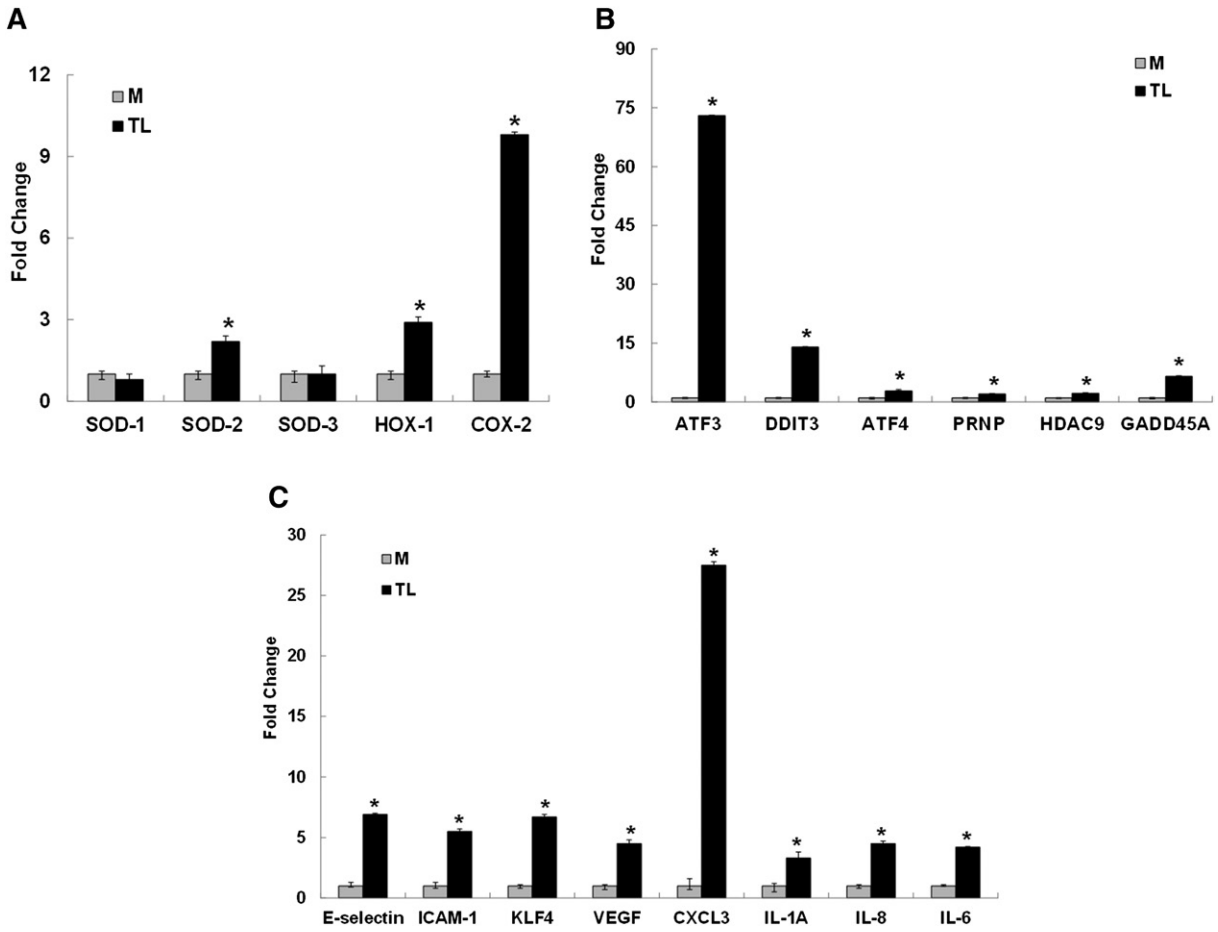

Fig. 3. TGRL lipolysis product-induced gene transcription determined by qRT-PCR. HBMECs were treated with media (M) or TGRL lipolysis products (TL, 150 mg/dl TGRLs plus 2 U/ml LPL) for 3 h. A: Oxidative stress genes: mitochondrial SOD-2, COX-2, and HOX-1; soluble SOD-1; and extracellular SOD-3. B: Stress response genes: ATF3, ATF4, DDIT3, PRNP, HDAC9, and GADD45A. C: Proinflammatory response genes: E-selectin, ICAM-1, KLF4, VEGF, CXCL3, IL-1α, IL-8, and IL-6. Expression of each gene was normalized to that of GAPDH, and fold change was calculated as the ratio of TL to media control. n = 3/treatment group, and results are expressed as means ± SEM. * $P \leq 0.05$ was considered significant (TL compared with M, L, or T).

the mitochondria, which corresponds with the mitochondrial injury visualized by electron microscopy. Although ROS production generated by TGRL lipolysis products is likely to be very complex, the major source of ROS production appears to be the mitochondria. We have shown caspase-9 and caspase-3/7 activity in HBMECs was increased by lipolysis products. Intracellular stress can induce apoptosis through the intrinsic cell death pathway. Intrinsic apoptosis is mitochondrion-centered cell death mediated by mitochondrial outer membrane permeabilization and results in apoptosome formation, activation of caspase-9, and subsequent activation of effector caspases, including caspase-3. During intrinsic cell death, stimulation of caspase-9 and effector caspases have sequential and distinct effects on mitochondria (49).

TGRL lipolysis products further induced increased transcription of a wide array of proinflammatory, stress response, and oxidative stress genes. This collection of cellular responses parallels that observed in our previous studies with aortic endothelial cells (22, 23, 27). As our previous work has demonstrated an important role for ATF3 in acute lipid-induced injury in aortic endothelium (22), we investigated the involvement of ATF3 in the brain microvascular endothelial cell responses to TGRL lipolysis products. We observed markedly upregulated ATF3 expression within 3 h of treatment, as well as increased nuclear accumulation of ATF3. ATF3 is a member of the ATF/cyclic-AMP response element-binding family of transcription factors characterized by the presence of a basic-region leucine zipper (50). Members of this transcription factor family share the ability to bind to the consensus sequence TGACGTCA located in the cyclic AMP response element of many different promoter regions (51, 52). ATF3 can act as either an activating or repressing transcription factor for many other genes and is therefore considered an adaptive-response gene. Previous studies have shown that depending on its dimeric state (homodimer versus heterodimer), upregulation of ATF3 can be pro- or anti-inflammatory (53–57).

We have recently shown that in human aortic endothelial cells, TGRL lipolysis product-stimulated ATF3 regulation proceeds via a complex cascade partially mediated by p-JNK transcription factor networks that are dependent on the rapid nuclear translocation of ATF3, heterodimer

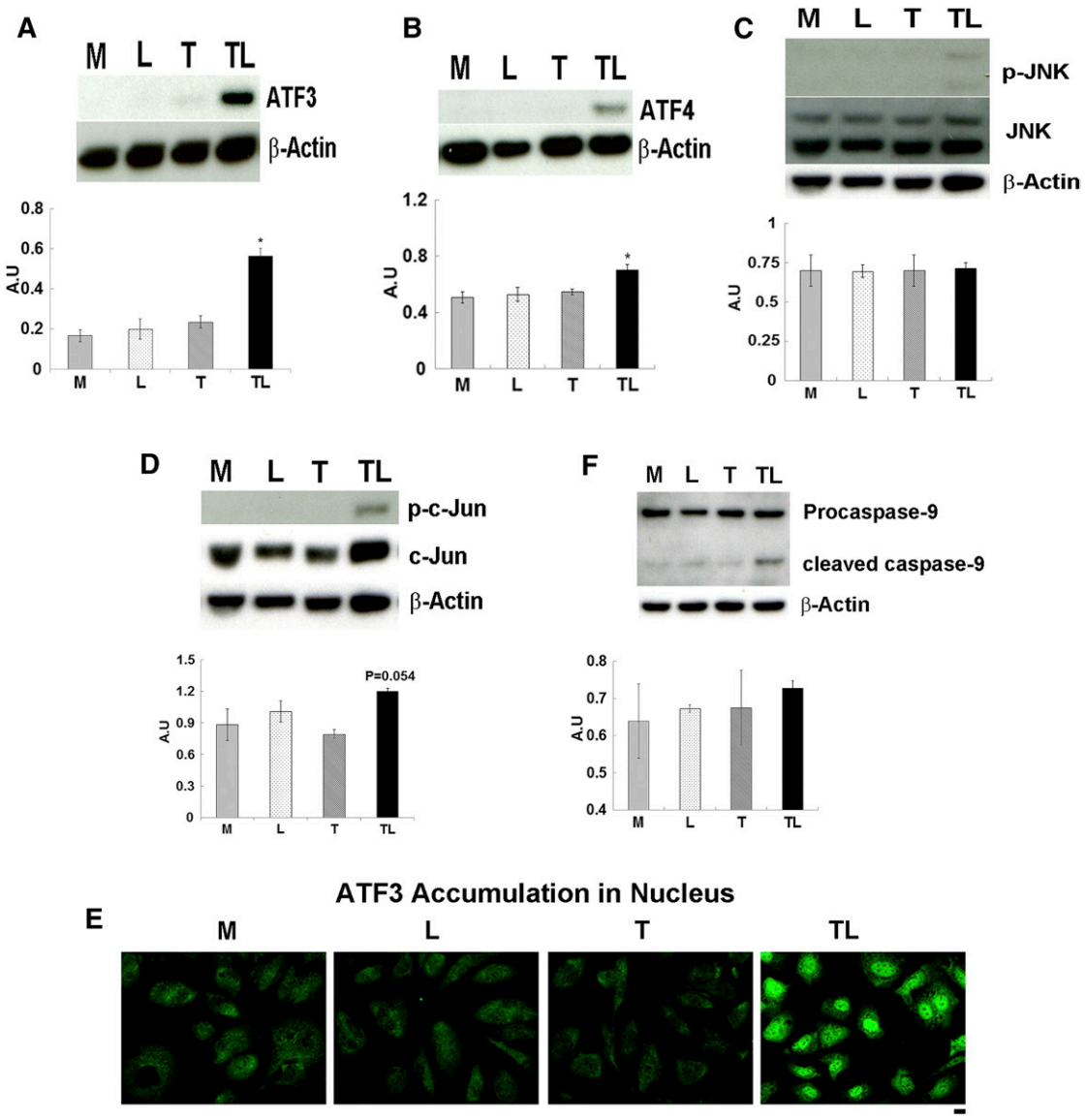

Fig. 4. TGRL lipolysis products increase ATF3, ATF4, p-JNK, p-c-Jun, and c-Jun protein expression. HBMECs were exposed to TGRL lipolysis products (T+L), media (M), LPL (L), or TGRLs (T) for 3 h. Cell lysates were analyzed by Western blotting and densitometry. A: Protein expression of ATF3 after the aforementioned treatments. B: Protein expression of ATF4. C: Protein expression of p-JNK. D: Protein expression of c-Jun and p-c-Jun. E: Immunofluorescence images of ATF3 demonstrate transition of cytosolic to nuclear accumulation of ATF3 following exposure to lipolysis products (bar = 40 μm). n = 5 coverslips/treatment group. F: Protein expression of cleaved caspase-9 (37 kDa). For A–D and F, n = 3, and $^{\#}P \leq 0.05$ for T+L compared with M, L, or T.

conformation, and formation of a p-c-Jun/ATF3 AP-1 binding complex (22). Our present work indicates the signaling mechanism underlying ATF3 activation in brain microvascular endothelium appears to be similarly complex but involves different players. We observed increased p-c-Jun and ATF3 protein levels, suggesting involvement of the same AP-1 binding complex. We also assessed the association between ATF3 upregulation and JNK phosphorylation. JNK belongs to a subset of MAPKs (a key cellular oxidative stress response pathway), thought to be upstream of the ATF3 signaling pathway, and has been previously shown to be an initiator of the ATF3 signaling cascade via transcriptional regulation (58). However, in contrast to our previous experiments in aortic endothelium, JNK activation was not upregulated in brain microvascular endothelium, and thus, TGRL lipolysis products likely activate ATF3 via different upstream factors in cerebrovascular inflammation.

In contrast to recently published studies showing that the anti-inflammatory effects of HDL were due to ATF3 dependent inhibition of TLR inflammatory pathways in macrophages (59), we have found ATF3 isoform, dimerization, and function to be dramatically different in different cell types and to be condition dependent. Herein, we describe the potential anti- and proinflammatory effects of ATF3, which at least in part rely on the dimerization of ATF3 pairs or quads. Our recent work examining single molecule cellular dynamics of ATF3 showed dramatic

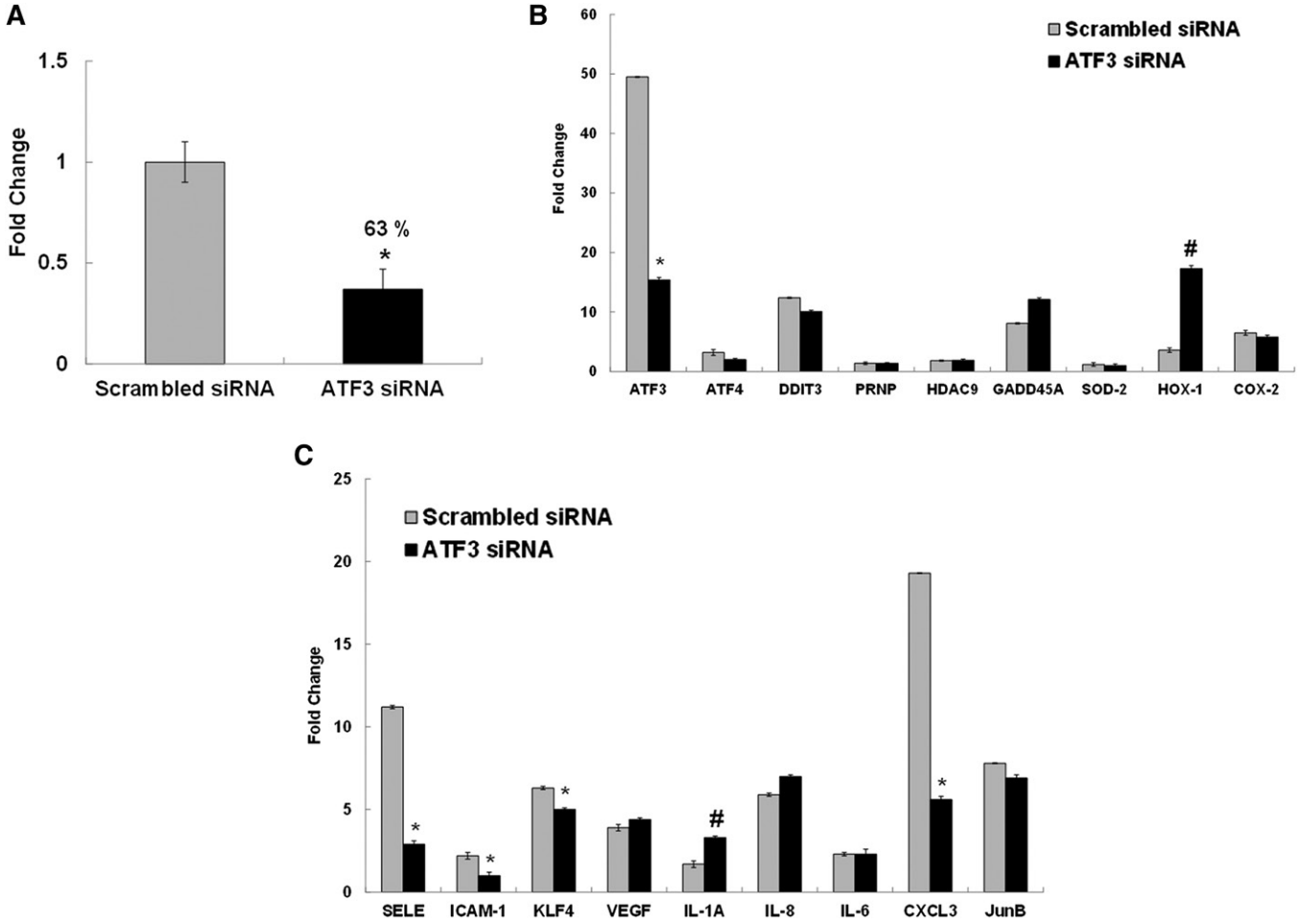

Fig. 5. Effect of ATF3 siRNA on TGRL lipolysis product-induced gene transcription. HBMECs were pretreated with siRNA 18 h prior to lipolysis product exposure for 3 h. A: mRNA was significantly knocked down after transfection with ATF3 siRNA for 18 h. B: Alterations in the transcription of ATF3, ATF4, DDIT3, PRNP, HDAC9, GADD45A, SOD-2, HOX-1, and COX-2. C: Alterations in the transcription of E-selectin, ICAM-1, KLF4, VEGF, IL-1α, IL-8, IL-6, CXCL3, and JunB. Expression of each gene was normalized to that of GAPDH and fold change was calculated by comparing TGRL lipolysis product-induced transcription between scrambled siRNA and ATF3 siRNA groups. n = 3/treatment group, and results are expressed as means ± SEM. * $P \leq 0.05$ (downregulated); # $P \leq 0.05$ (upregulated).

dimerization of ATF3 pairs that promote a proinflammatory cellular cascade (30). Further, our prior studies show that in response to lipids, ATF3 expression in monocytes (60), macrophages, astrocytes, and microglia is much reduced compared with ATF3 expression in endothelial cells.

Additionally, we observed upregulated gene transcription and increased protein levels of ATF4 in HBMECs in response to TGRL lipolysis products. siRNA knockdown experiments further elucidated the involvement of ATF3 and ATF4 transcription factors in our model, as pretreatment with ATF3 siRNA resulted in decreased gene transcription and protein expression of ATF3 and ATF4 but caused an increase in p-c-Jun. ATF3 siRNA also attenuated the TGRL lipolysis product-induced transcription of most of the inflammatory markers investigated, suggesting activation of this transcriptional pathway proceeds through c-Jun phosphorylation and an ATF3/ATF4 binding complex. However, ATF3 knockdown increased transcription of the oxidative stress gene HOX-1. Thus, although ATF3 appears to be a primary regulator of inflammatory gene transcription, other regulatory factors are responsible for modulation of adaptive oxidative stress responses following lipotoxic injury.

There is now significant clinical and epidemiologic data available pointing to the strong association of hyperlipidemia, as well as obesity, diabetes, and hypertension, in the development and possible causation of dementia. This has been reviewed in our prior publication (61). Unfortunately, reversal or prevention of dementia with hypolipidemic therapies has not been adequately tested. Interestingly, ATF3-mediated neuroinflammation in response to chronic lipid-induced injury appears to be a regional process. Previous studies have primarily focused on hypothalamic lipotoxicity, with much less emphasis paid to cortical and cerebral lipotoxicity (62, 63). Our in vivo studies revealed elevated ATF3 expression in brain vasculature that was confined to the cerebellum and the hippocampus, but did not extend to the temporal and frontal lobes, supporting the notion that in response to a lipotoxic insult to the brain, ATF3 upregulation may indeed proceed in

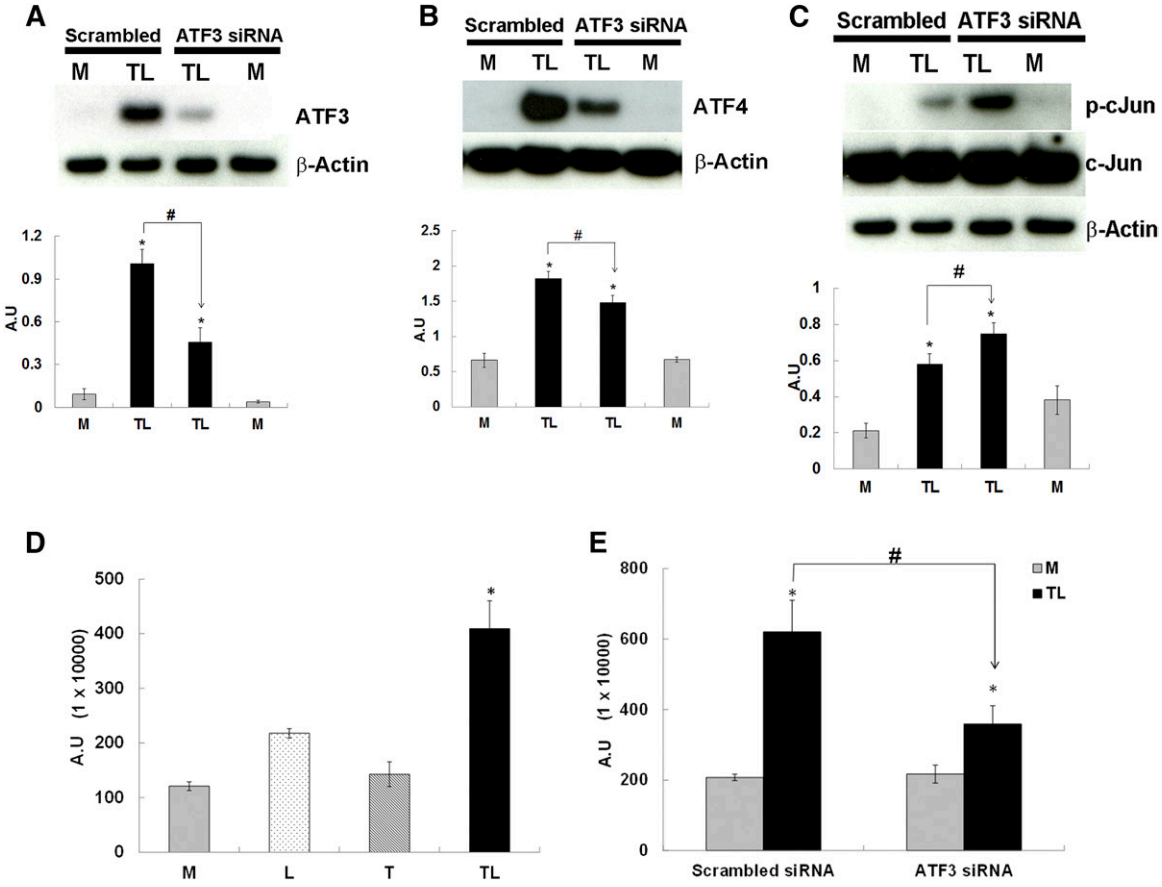

Fig. 6. Effect of ATF3 siRNA on TGRL lipolysis product-induced protein expression and apoptosis. HBMECs were transfected with ATF3 siRNA for 18 h and treated with TGRL lipolysis products (TL) for 3 h. A: Alterations in ATF3 protein expression. B: Downregulation of ATF4 protein expression. C: Upregulation of p-c-Jun and c-Jun. For A–C, Western blot and densitometry quantification were performed with n = 3/treatment group. *$P \leqslant 0.05$ for comparisons between scrambled siRNA exposed to media (M) and TGRL lipolysis products (TL), or ATF3 siRNA exposed to M and TL. $^{\#}P \leqslant 0.05$ denotes the difference between TL with scrambled siRNA and TL with ATF3 siRNA. D: Caspase-3/7 activity was significantly increased with TGRL lipolysis products (TL) after 3 h of incubation. * = TL compared with media (M), LPL (L), or TGRLs (T) alone. E: Caspase-3/7 activity significantly decreased in cells transfected with ATF3 siRNA. n = 7/treatment group. * $P \leqslant 0.05$ (TL compared with M), and $^{\#}P \leqslant 0.05$ (TL with scrambled compared with ATF3 siRNA).

a stimulus- and region-specific manner. Our studies have relevance to disease in humans as the hippocampus is a major target region of the brain involved in Alzheimer's disease pathology. With regard to cerebellar expression of ATF3 and cognitive function, a number of recent publications have indicated that the cerebellum may be involved with cognitive function (64). In addition, the cerebellum is hypothesized to play a key role in the development of vascular dementia (65). Thus, due to its adaptive function, ATF3 may serve as a mediator of protective cellular responses to help neural tissues recover from injury following a lipotoxic insult, or it may induce increased damage. Further studies are needed to clarify ATF3's regional role in the brain in response to chronic hyperlipidemic injury.

ApoE$^{-/-}$ mice were used for in vivo experiments, which is an established model for vascular inflammation and vascular atherosclerotic lesions. ApoE plays a central role in lipoprotein metabolism and is required for the efficient clearance of diet-derived chylomicrons and liver-derived VLDL remnants (66). Thus, mice lacking apoE (apoE$^{-/-}$) have elevated levels of VLDL (a subclass of TGRLs), LDL, and fatty acids they provided a practical model of hyperlipidemia and atherosclerosis. Moreover, apoE$^{-/-}$ mice serve as an appropriate model for studying pathogenic oxidative mechanisms influencing risk and progression of Alzheimer's disease (67, 68). In addition, postprandial apoE isoform and conformational changes associated with VLDL dramatically modulate vascular inflammation. Our published studies indicate that after every meal, VLDL lipolysis products increase VLDL particle fluidity, which mediates expansion of apoE4 on the VLDL particle. VLDL fluidity is increased causing apoE4 associated with VLDL to assume a more expanded conformation, potentially enhancing the pathogenicity of apoE4 in vascular tissue inflammation (34, 69). Furthermore, lipoprotein hydrolysis is less efficient in the apoE$^{-/-}$ mouse, which results in decreased fatty acid release by lipolysis; fatty acids are a major component of TGRL lipolysis products. However, fatty acids levels are also elevated in blood of apoE$^{-/-}$ mice through other mechanisms, and the elevated fatty acids may directly contribute to the lipotoxic response in the neurovascular unit.

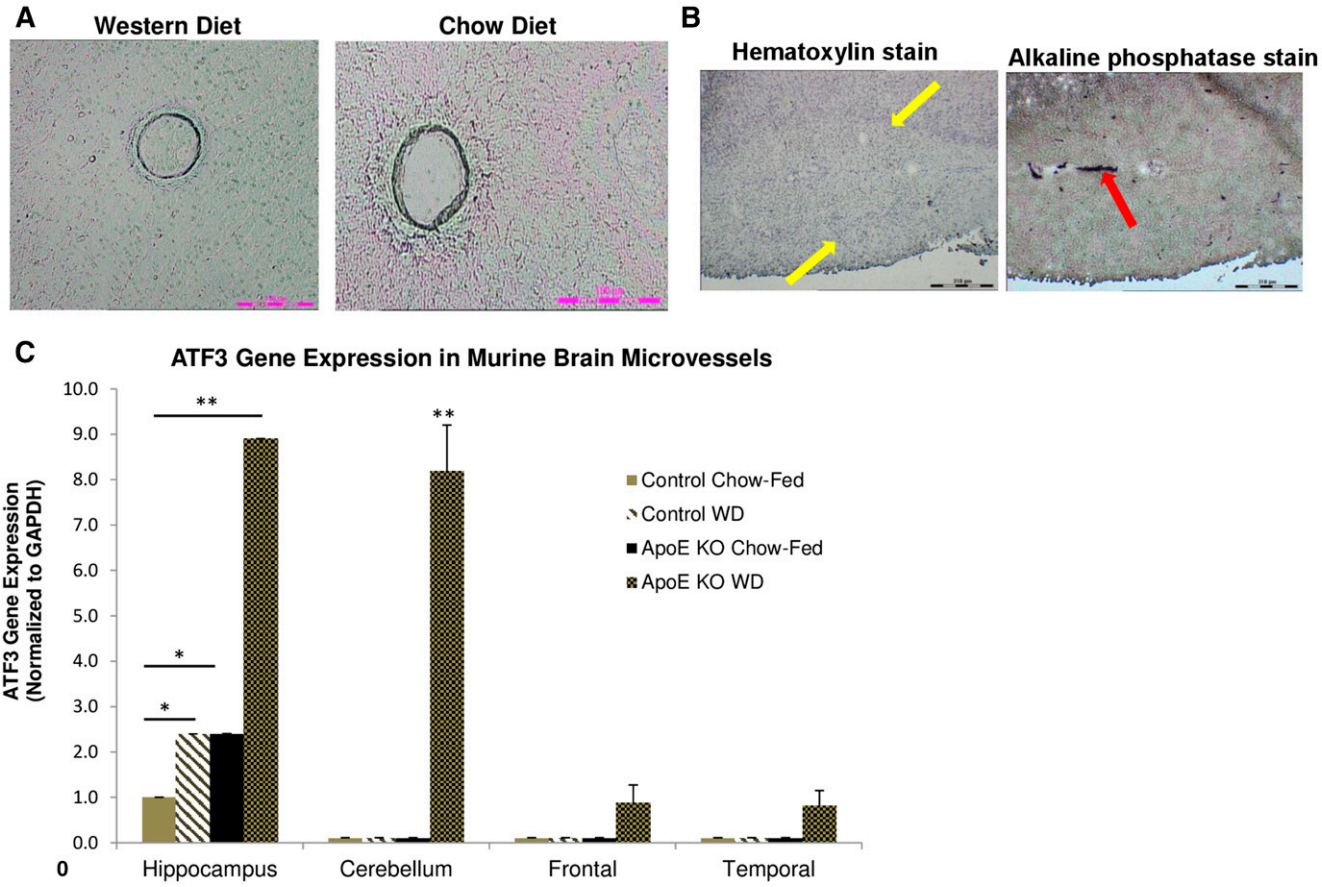

Fig. 7. A: Representative images of brain microvessels dissected by LCM. Microvessels were identified in brain sections (8 μm) of WD-fed apoE$^{-/-}$ and chow-fed apoE$^{-/-}$ male mice, and the entire vessel wall subjected to LCM. RNA was isolated, amplified, and subjected to gene expression analysis by qRT-PCR. The figure shows representative brain microvessels (arteriole, 100 μm lumen diameter) selected for LCM from WD-fed apoE$^{-/-}$ mice (left-hand panel) and chow-fed apoE$^{-/-}$ mice (right-hand panel; scale bar = 100 μm). B: Representative images of hippocampal neurons and brain microvessels dissected by LCM. Neurons and microvessels in the hippocampus (8 μm sections) of chow-fed apoE$^{-/-}$ mice were stained with hematoxylin (left panel, yellow arrows). Endothelium (shown in longitudinal section of a brain microvessel) was confirmed with alkaline phosphatase staining (right panel, red arrow) with BCIP/NBT substrate. C: Increased expression of ATF3 in microvessels from the hippocampus and the cerebellar brain regions of WD-fed apoE$^{-/-}$ mice. ApoE$^{-/-}$ (n = 5 to 7) and control C57BL/6J (n = 5 to 7) mice were fed a typical WD or chow for 6–8 weeks, after which hippocampus, cerebellum, frontal lobe, and temporal lobe brain sections were collected. LCM was used to isolate brain microvessels from each separate brain region. Total RNA was isolated, amplified, and used for qRT-PCR analysis of ATF3 gene transcription. Expression levels were normalized to GAPDH and expressed as means ± SEM. ** $P \leq 0.001$ WD-fed apoE$^{-/-}$ compared with all other groups. * $P \leq 0.05$ for WD-fed control compared with chow-fed control mice, and for chow-fed apoE$^{-/-}$ compared with chow-fed control mice.

In summary, we demonstrated TGRL lipolysis products cause lipotoxic brain microvascular endothelial injury by increasing mitochondrial superoxide radical and pro-apoptotic cascades, activating ATF3-mediated inflammatory pathways and inducing oxidative stress pathways (**Fig. 8**). Our results also show significantly upregulated transcription of ATF3 in hippocampal and cerebellar vessels in a chronic model of lipid-induced injury, further establishing ATF3's role in a key endothelial regulatory pathway that mediates lipotoxicity (22) and suggesting ATF3 may be a key response gene following acute or chronic lipid injury in vivo and in vitro. Although ATF3 is known to be regulated by a number of oncogenic, infectious, and cellular stress responses, we establish a previously undefined role for lipids, specifically lipolysis products of TGRLs and the high-fat WD, in inducing ATF3 expression in the cerebrovasculature. As such, ATF3 may reside at an important intersection between dietary lipids and detrimental cellular responses in the brain microvasculature and contribute to the dysfunction characteristic of VCI. ATF3 thus may be a candidate gene target for future therapeutics aimed at combating cerebrovascular injury.

LCM was conducted at the Cellular and Molecular Imaging core facility at the University of California, Davis Center for Health and the Environment. The authors thank Cris Warford, Camille Schilling, and Sindhu Addepalli for technical assistance with the LCM studies. The authors would also like to thank the human subjects who donated blood for these studies, as well as the staff of the Western Human Nutrition Research Center and the Ragle Human Nutrition Center at the University of California, Davis for donating their valuable time and expertise to this study.

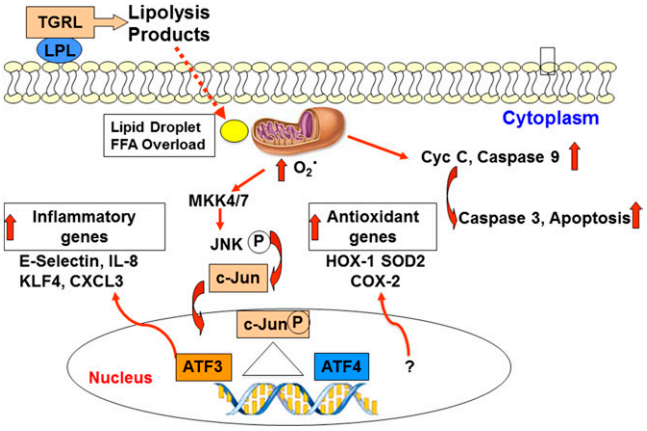

Fig. 8. Proposed schematic of signaling cascade for lipid and lipolysis product-induced mitochondrial stress responses and ATF3. TGRL lipolysis products increase superoxide radical generation and lipid droplet formation. Activation of stress signaling pathways causes release of cytochrome C from mitochondria and subsequent activation of proapoptotic caspase-9. Phosphorylation of c-Jun results in upregulation of ATF3 and ATF4 gene transcription and protein expression and induces inflammatory gene transcription responses. Parallel activation of oxidative stress gene transcription also occurs in response to TGRL lipolysis products.

REFERENCES

1. Plassman, B. L., K. M. Langa, G. G. Fisher, S. G. Heeringa, D. R. Weir, M. B. Ofstedal, J. R. Burke, M. D. Hurd, G. G. Potter, W. L. Rodgers, et al. 2007. Prevalence of dementia in the United States: the aging, demographics, and memory study. *Neuroepidemiology.* **29:** 125–132.
2. Gorelick, P. B., A. Scuteri, S. E. Black, C. Decarli, S. M. Greenberg, C. Iadecola, L. J. Launer, S. Laurent, O. L. Lopez, D. Nyenhuis, et al. 2011. Vascular contributions to cognitive impairment and dementia: a statement for healthcare professionals from the American Heart Association/American Stroke Association. *Stroke.* **42:** 2672–2713.
3. de Lorgeril, M., P. Salen, J-L. Martin, N. Mamelle, I. Monjaud, P. Touboul, and J. Delaye. 1996. Effect of a Mediterranean type of diet on the rate of cardiovascular complications in patients with coronary artery disease insights into the cardioprotective effect of certain nutriments. *J. Am. Coll. Cardiol.* **28:** 1103–1108.
4. de Lorgeril, M., P. Salen, J-L. Martin, I. Monjaud, J. Delaye, and N. Mamelle. 1999. Mediterranean diet, traditional risk factors, and the rate of cardiovascular complications after myocardial infarction: final report of the Lyon Diet Heart Study. *Circulation.* **99:** 779–785.
5. Menotti, A., D. Kromhout, H. Blackburn, F. Fidanza, R. Buzina, and A. Nissinen; Seven Countries Study Research Group. 1999. Food intake patterns and 25-year mortality from coronary heart disease: cross-cultural correlations in the Seven Countries Study. *Eur. J. Epidemiol.* **15:** 507–515.
6. Singh, R. B., G. Dubnov, M. A. Niaz, S. Ghosh, R. Singh, S. S. Rastogi, O. Manor, D. Pella, and E. M. Berry. 2002. Effect of an Indo-Mediterranean diet on progression of coronary artery disease in high risk patients (Indo-Mediterranean Diet Heart Study): a randomised single-blind trial. *Lancet.* **360:** 1455–1461.
7. Yusuf, S., S. Hawken, S. Ôunpuu, T. Dans, A. Avezum, F. Lanas, M. McQueen, A. Budaj, P. Pais, J. Varigos, et al. 2004. Effect of potentially modifiable risk factors associated with myocardial infarction in 52 countries (the INTERHEART study): case-control study. *Lancet.* **364:** 937–952.
8. Hall, W. L. 2009. Dietary saturated and unsaturated fats as determinants of blood pressure and vascular function. *Nutr. Res. Rev.* **22:** 18–38.
9. Takechi, R., S. Galloway, M. M. Pallebage-Gamarallage, V. Lam, and J. C. Mamo. 2010. Dietary fats, cerebrovasculature integrity and Alzheimer's disease risk. *Prog. Lipid Res.* **49:** 159–170.
10. Engelhart, M. J., M. I. Geerlings, A. Ruitenberg, J. C. van Swieten, A. Hofman, J. C. M. Witteman, and M. M. B. Breteler. 2002. Diet and risk of dementia: does fat matter? The Rotterdam Study. *Neurology.* **59:** 1915–1921.
11. Laitinen, M. H., T. Ngandu, S. Rovio, E. L. Helkala, U. Uusitalo, M. Viitanen, A. Nissinen, J. Tuomilehto, H. Soininen, and M. Kivipelto. 2006. Fat intake at midlife and risk of dementia and Alzheimer's disease: a population-based study. *Dement. Geriatr. Cogn. Disord.* **22:** 99–107.
12. Luchsinger, J. A., and R. Mayeux. 2004. Dietary factors and Alzheimer's disease. *Lancet Neurol.* **3:** 579–587.
13. Morris M. C., D. A. Evans, J. L. Bienias, C. C. Tangney, D. A. Bennett, N. Aggarwal, J. Schneider, and R. S. Wilson. 2003. Dietary fats and the risk of incident Alzheimer disease. *Arch. Neurol.* **60:** 194–200.
14. Solfrizzi, V., A. D'Introno, A. M. Colacicco, C. Capurso, A. Del Parigi, S. Capurso, A. Gadaleta, A. Capurso, and F. Panza. 2005. Dietary fatty acids intake: possible role in cognitive decline and dementia. *Exp. Gerontol.* **40:** 257–270.
15. Grammas, P. 2011. Neurovascular dysfunction, inflammation and endothelial activation: implications for the pathogenesis of Alzheimer's disease. *J. Neuroinflammation.* **8:** 26.
16. Mizuno, Y., R. F. Jacob, and R. P. Mason. 2011. Inflammation and the development of atherosclerosis. *J. Atheroscler. Thromb.* **18:** 351–358.
17. Goldberg, I. J., Y. Kako, and E. P. Lutz. 2000. Responses to eating: lipoproteins, lipolytic products and atherosclerosis. *Curr. Opin. Lipidol.* **11:** 235–241.
18. Goldberg, I. J., and M. Merkel. 2001. Lipoprotein lipase: physiology, biochemistry, and molecular biology. *Front. Biosci.* **6:** D388–D405.
19. López-Miranda, J., P. Pérez-Martínez, C. Marín, J. A. Moreno, P. Gómez, and F. Pérez-Jiménez. 2006. Postprandial lipoprotein metabolism, genes and risk of cardiovascular disease. *Curr. Opin. Lipidol.* **17:** 132–138.
20. Merkel, M., R. H. Eckel, and I. J. Goldberg. 2002. Lipoprotein lipase: genetics, lipid uptake, and regulation. *J. Lipid Res.* **43:** 1997–2006.
21. Otarod, J. K., and I. J. Goldberg. 2004. Lipoprotein lipase and its role in regulation of plasma lipoproteins and cardiac risk. *Curr. Atheroscler. Rep.* **6:** 335–342.
22. Aung, H. H., M. W. Lame, K. Gohil, C. I. An, D. W. Wilson, and J. C. Rutledge. 2013. Induction of ATF3 gene network by triglyceride-rich lipoprotein lipolysis products increases vascular apoptosis and inflammation. *Arterioscler. Thromb. Vasc. Biol.* **33:** 2088–2096.
23. Eiselein, L., D. W. Wilson, M. W. Lame, and J. C. Rutledge. 2007. Lipolysis products from triglyceride-rich lipoproteins increase endothelial permeability, perturb zonula occludens-1 and F-actin, and induce apoptosis. *Am. J. Physiol. Heart Circ. Physiol.* **292:** H2745–H2753.
24. Hennig, B., B. H. Chung, B. A. Watkins, and A. Alvarado. 1992. Disruption of endothelial barrier function by lipolytic remnants of triglyceride-rich lipoproteins. *Atherosclerosis.* **95:** 235–247.
25. Motojima, K., K. Azuma, Y. Kitahara, K. Miura, T. Mita, T. Hirose, Y. Fujitani, R. Kawamori, and H. Watada. 2008. Repetitive postprandial hypertriglyceridemia induces monocyte adhesion to aortic endothelial cells in Goto-Kakizaki rats. *Endocr. J.* **55:** 373–379.
26. Rutledge, J. C., A. E. Mullick, G. Gardner, and I. J. Goldberg. 2000. Direct visualization of lipid deposition and reverse lipid transport in a perfused artery: roles of VLDL and HDL. *Circ. Res.* **86:** 768–773.
27. Wang, L., R. Gill, T. L. Pedersen, L. J. Higgins, J. W. Newman, and J. C. Rutledge. 2009. Triglyceride-rich lipoprotein lipolysis releases neutral and oxidized FFAs that induce endothelial cell inflammation. *J. Lipid Res.* **50:** 204–213.
28. Wang, L., A. R. Sapuri-Butti, H. H. Aung, A. N. Parikh, and J. C. Rutledge. 2008. Triglyceride-rich lipoprotein lipolysis increases aggregation of endothelial cell membrane microdomains and produces reactive oxygen species. *Am. J. Physiol. Heart Circ. Physiol.* **295:** H237–H244.
29. Wheeler-Jones, C. P. 2007. Chylomicron remnants: mediators of endothelial dysfunction? *Biochem. Soc. Trans.* **35:** 442–445.
30. Yahiatène, I., H. H. Aung, D. W. Wilson, and J. C. Rutledge. 2014. Single-molecule quantification of lipotoxic expression of activating transcription factor 3. *Phys. Chem. Chem. Phys.* **16:** 21595–21601.
31. den Hartigh, L. J., J. E. Connolly-Rohrbach, S. Fore, T. R. Huser, and J. C. Rutledge. 2010. Fatty acids from very low-density lipoprotein lipolysis products induce lipid droplet accumulation in human monocytes. *J. Immunol.* **184:** 3927–3936.
32. Hyson, D. A., T. G. Paglieroni, T. Wun, and J. C. Rutledge. 2002. Postprandial lipemia is associated with platelet and monocyte activation

and increased monocyte cytokine expression in normolipemic men. *Clin. Appl. Thromb. Hemost.* **8:** 147–155.
33. Motton, D. D., N. Mackman, R. E. Tilley, and J. C. Rutledge. 2005. Postprandial elevation of tissue factor antigen in the blood of healthy adults. *Thromb. Haemost.* **94:** 504–509.
34. Tetali, S. D., M. S. Budamagunta, C. Simion, L. J. den Hartigh, T. Kálai, K. Hideg, D. M. Hatters, K. H. Weisgraber, J. C. Voss, and J. C. Rutledge. 2010. VLDL lipolysis products increase VLDL fluidity and convert apolipoprotein E4 into a more expanded conformation. *J. Lipid Res.* **51:** 1273–1283.
35. Dikalov, S. I., I. A. Kirilyuk, M. Voinov, and I. A. Grigor'ev. 2011. EPR detection of cellular and mitochondrial superoxide using cyclic hydroxylamines. *Free Radic. Res.* **45:** 417–430.
36. Livak, K. J., and T. D. Schmittgen. 2001. Analysis of relative gene expression data using real-time quantitative PCR and the 2(-Delta Delta C(T)) Method. *Methods.* **25:** 402–408.
37. Breslow, J. L. 1996. Mouse models of atherosclerosis. *Science.* **272:** 685–688.
38. Jawień, J., P. Nastalek, and R. Korbut. 2004. Mouse models of experimental atherosclerosis. *J. Physiol. Pharmacol.* **55:** 503–517.
39. Stary, H. C., D. H. Blankenhorn, A. B. Chandler, S. Glagov, W. Insull, Jr., M. Richardson, M. E. Rosenfeld, S. A. Schaffer, C. J. Schwartz, W. D. Wagner, et al. 1992. A definition of the intima of human arteries and of its atherosclerosis-prone regions. A report from the Committee on Vascular Lesions of the Council on Arteriosclerosis, American Heart Association. *Circulation.* **85:** 391–405.
40. Stary, H. C., A. B. Chandler, R. E. Dinsmore, V. Fuster, S. Glagov, W. Insull, Jr., M. E. Rosenfeld, C. J. Schwartz, W. D. Wagner, and R. W. Wissler. 1995. A definition of advanced types of atherosclerotic lesions and a histological classification of atherosclerosis. A report from the Committee on Vascular Lesions of the Council on Arteriosclerosis, American Heart Association. *Circulation.* **92:** 1355–1374.
41. Stary, H. C., A. B. Chandler, S. Glagov, J. R. Guyton, W. Insull, Jr., M. E. Rosenfeld, S. A. Schaffer, C. J. Schwartz, W. D. Wagner, and R. W. Wissler. 1994. A definition of initial, fatty streak, and intermediate lesions of atherosclerosis. A report from the Committee on Vascular Lesions of the Council on Arteriosclerosis, American Heart Association. *Circulation.* **89:** 2462–2478.
42. Ball, H. J., B. McParland, C. Driussi, and N. H. Hunt. 2002. Isolating vessels from the mouse brain for gene expression analysis using laser capture microdissection. *Brain Res. Brain Res. Protoc.* **9:** 206–213.
43. Aung, H. H., A. Tsoukalas, J. C. Rutledge, and I. Tagkopoulos. 2014. A systems biology analysis of brain microvascular endothelial cell lipotoxicity. *BMC Syst. Biol.* **8:** 80.
44. Kalmijn, S. 2000. Fatty acid intake and the risk of dementia and cognitive decline: a review of clinical and epidemiological studies. *J. Nutr. Health Aging.* **4:** 202–207.
45. Solfrizzi, V., V. Frisardi, C. Capurso, A. D'Introno, A. M. Colacicco, G. Vendemiale, A. Capurso, and F. Panza. 2010. Dietary fatty acids in dementia and predementia syndromes: epidemiological evidence and possible underlying mechanisms. *Ageing Res. Rev.* **9:** 184–199.
46. Garbarino, J., and S. L. Sturley. 2009. Saturated with fat: new perspectives on lipotoxicity. *Curr. Opin. Clin. Nutr. Metab. Care.* **12:** 110–116.
47. Schaffer, J. E. 2003. Lipotoxicity: when tissues overeat. *Curr. Opin. Lipidol.* **14:** 281–287.
48. Unger, R. H., and L. Orci. 2002. Lipoapoptosis: its mechanism and its diseases. *Biochim. Biophys. Acta.* **1585:** 202–212.
49. Galluzzi, L., I. Vitale, J. M. Abrams, E. S. Alnemri, E. H. Baehrecke, M. V. Blagosklonny, T. M. Dawson, V. L. Dawson, W. S. El-Deiry, S. Fulda, et al. 2012. Molecular definitions of cell death subroutines: recommendations of the Nomenclature Committee on Cell Death 2012. *Cell Death Differ.* **19:** 107–120.
50. Thompson, M. R., D. Xu, and B. R. Williams. 2009. ATF3 transcription factor and its emerging roles in immunity and cancer. *J. Mol. Med..* **87:** 1053–1060.
51. Deutsch, P. J., J. P. Hoeffler, J. L. Jameson, J. C. Lin, and J. F. Habener. 1988. Structural determinants for transcriptional activation by cAMP-responsive DNA elements. *J. Biol. Chem.* **263:** 18466–18472.
52. Montminy, M. R., and L. M. Bilezikjian. 1987. Binding of a nuclear protein to the cyclic-AMP response element of the somatostatin gene. *Nature.* **328:** 175–178.
53. Gilchrist, M., V. Thorsson, B. Li, A. G. Rust, M. Korb, J. C. Roach, K. Kennedy, T. Hai, H. Bolouri, and A. Aderem. 2006. Systems biology approaches identify ATF3 as a negative regulator of Toll-like receptor 4. *Nature.* **441:** 173–178. [Erratum. 2008. *Nature.* 451: 1022.]
54. Hsu, J. C., T. Laz, K. L. Mohn, and R. Taub. 1991. Identification of LRF-1, a leucine-zipper protein that is rapidly and highly induced in regenerating liver. *Proc. Natl. Acad. Sci. USA.* **88:** 3511–3515.
55. Khuu, C. H., R. M. Barrozo, T. Hai, and S. L. Weinstein. 2007. Activating transcription factor 3 (ATF3) represses the expression of CCL4 in murine macrophages. *Mol. Immunol.* **44:** 1598–1605.
56. Whitmore, M. M., A. Iparraguirre, L. Kubelka, W. Weninger, T. Hai, and B. R. G. Williams. 2007. Negative regulation of TLR-signaling pathways by activating transcription factor-3. *J. Immunol.* **179:** 3622–3630.
57. Zmuda, E. J., M. Viapiano, S. T. Grey, G. Hadley, A. Garcia-Ocana, and T. Hai. 2010. Deficiency of Atf3, an adaptive-response gene, protects islets and ameliorates inflammation in a syngeneic mouse transplantation model. *Diabetologia.* **53:** 1438–1450.
58. Inoue, K., T. Zama, T. Kamimoto, R. Aoki, Y. Ikeda, H. Kimura, and M. Hagiwara. 2004. TNFalpha-induced ATF3 expression is bi-directionally regulated by the JNK and ERK pathways in vascular endothelial cells. *Genes Cells.* **9:** 59–70.
59. De Nardo, D., L. I. Labzin, H. Kono, R. Seki, S. V. Schmidt, M. Beyer, D. Xu, S. Zimmer, C. Lahrmann, F. A. Schildberg, et al. 2014. High-density lipoprotein mediates anti-inflammatory reprogramming of macrophages via the transcriptional regulator ATF3. *Nat. Immunol.* **15:** 152–160.
60. den Hartigh, L. J., R. Altman, J. E. Norman, and J. C. Rutledge. 2014. Postprandial VLDL lipolysis products increase monocyte adhesion and lipid droplet formation via activation of ERK2 and NFkappaB. *Am. J. Physiol. Heart Circ. Physiol.* **306:** H109–H120.
61. Altman, R., and J. C. Rutledge. 2010. The vascular contribution to Alzheimer's disease. *Clin. Sci. (Lond.).* **119:** 407–421.
62. Le Stunff, H., N. Coant, S. Migrenne, and C. Magnan. 2013. Targeting lipid sensing in the central nervous system: new therapy against the development of obesity and type 2 diabetes. *Expert Opin. Ther. Targets.* **17:** 545–555.
63. Martínez de Morentin, P. B., L. Varela, J. Fernø, R. Nogueiras, C. Diéguez, and M. López. 2010. Hypothalamic lipotoxicity and the metabolic syndrome. *Biochim. Biophys. Acta.* **1801:** 350–361.
64. Wang, S. S., A. D. Kloth, and A. Badura. 2014. The cerebellum, sensitive periods, and autism. *Neuron.* **83:** 518–532.
65. Sui, R., and L. Zhang. 2012. Cerebellar dysfunction may play an important role in vascular dementia. *Med. Hypotheses.* **78:** 162–165.
66. Mahley, R. W. 1988. Apolipoprotein E: cholesterol transport protein with expanding role in cell biology. *Science.* **240:** 622–630.
67. Choi, J., M. J. Forster, S. R. McDonald, S. T. Weintraub, C. A. Carroll, and R. W. Gracy. 2004. Proteomic identification of specific oxidized proteins in ApoE-knockout mice: relevance to Alzheimer's disease. *Free Radic. Biol. Med.* **36:** 1155–1162.
68. Corder, E. H., A. M. Saunders, W. J. Strittmatter, D. E. Schmechel, P. C. Gaskell, G. W. Small, A. D. Roses, J. L. Haines, and M. A. Pericak-Vance. 1993. Gene dose of apolipoprotein E type 4 allele and the risk of Alzheimer's disease in late onset families. *Science.* **261:** 921–923.
69. den Hartigh, L. J., R. Altman, R. Hutchinson, J. Petrlova, M. S. Budamagunta, S. D. Tetali, J. O. Lagerstedt, J. C. Voss, and J. C. Rutledge. 2012. Postprandial apoE isoform and conformational changes associated with VLDL lipolysis products modulate monocyte inflammation. *PLoS One.* **7:** e50513.